ARTICLE

Side-Chain Functionalized Supramolecular Helical Brush Copolymers

Received 00th January 20xx,
Accepted 00th January 20xx

DOI: 10.1039/x0xx00000x

Ru Deng,[a] Chengyuan Wang,[a] Margarita Milton,[a] Danni Tang,[a] Andrew D. Hollingsworth,[b] and Marcus Weck*[a]

We report poly(isocyanide)-based random copolymers (***co*-PIC**) featuring alkoxycarbonyl-based side-chains synthesized via the metal-catalyzed controlled polymerization of chiral and achiral isocyanide monomers. The pyridine-functionalized achiral monomer provides functional sites while the chiral monomer drives the formation of a one-handed preferred helix. The side-chain functionalized helical polymer undergoes self-assembly with palladated pincer ligands, as evidenced by ^{1}H NMR and UV-Vis spectroscopies. Circular dichroism (CD) spectroscopy confirms that the side-chain self-assembly does not affect the backbone helicity. We construct supramolecular helical brush copolymers via the metal coordination of the ***co*-PIC** backbone with telechelic poly(styrene)s. ^{1}H NMR and UV-Vis spectroscopies confirm the metal coordination, and CD measurements suggest that the backbone retains its helical conformation. Additionally, viscometry measurements verify the formation of high molecular weight polymers while dynamic light scattering confirms the increasing hydrodynamic radii of the resulting supramolecular brush copolymers. Our methodology constructs complex 3D materials with fully synthetic, secondary structure containing building blocks. We view this as a platform for building architecturally controlled 3D supramolecular materials with high degrees of complexity.

Introduction

Synthetic polymers that mimic the structure and functionality of biological macromolecules have led to remarkable achievements in polymer science.[1–3] These synthetic systems simulate the folding, chain collapse, and inter/intra-chain interactions of biomacromolecules to form various topologically diverse structures,[4–6] and induce enzymatic functions including catalysis, recognition, and long-range ordered molecular machines.[7–9] Despite these advances in structural complexity, the scope of artificial building blocks to build highly ordered polymeric structures remains limited. Compared to amino acid-based foldamers, non-amide polymeric backbones enable the utilization of more diverse sets of monomers and polymerization methods.[10–13] We have introduced the directed assembly of non-amide based polymers bearing secondary structures, including helices, sheets, and coils.[14–17] This approach uses multiple molecular recognition pairs, allowing for precise spatial control over building blocks thereby expanding our capability to achieve complexity and may lead to the fabrication of functional materials.[18]

The incorporation of secondary structure elements into three-dimensional polymeric ensembles displays intriguing material properties that are not achievable through the 2D linear assembly. Maeda and co-workers reported the "sergeant and soldier effect" of helical brush copolymers with poly(phenylacetylene) backbones and poly(phenyl isocyanide) pendants, showing long-range chiral amplifications.[19,20] Baumgartner *et al*. reported a polypeptide-based brush copolymer where the spatial arrangements of helical side-chains catalyzed their own formations.[21] The incorporation of helical segments in complex polymeric architectures has found various applications including size separation, catalysis, circularly polarized luminescence and chiral recognition.[22–27] Elacqua *et al.* brought β-sheet mimicking poly(*p*-phenylenevinylene) block copolymers to a new level of complexity.[28] The stacked antiparallel sheets with up to five turns demonstrated that the increasing folds of the polymers induced a higher degree of order. These examples prove that 3D spatial assembly will be the key to fabricating the next generation of functional materials.

Compared to building 3D complex materials via covalent linkages, fabricating 3D architectures through noncovalent interactions remains challenging. Unlike head-to-tail linear assemblies, 3D spatial control requires polymers with multiple molecular recognition units functionalized on the side-chains.[29] This class of polymers possess unique properties including self-healing capabilities,[30] enhanced mechanical properties,[31] and the ability to build dynamic polymer networks.[32] Using a single strand collapse strategy, Barner-Kowollik and Meijer produced block copolymers with multiple recognition units. Under high dilution, these polymers fold into single-chain nanoparticles (SCNPs) driven by interchain helical stack and noncovalent

[a]*Department of Chemistry and Molecular Design Institute, New York University, New York, NY 10003, USA. E-mail: marcus.weck@nyu.edu*
[b]*Department of Physics and Center for Soft Matter Research, New York University, New York, NY 10003, USA.*
Electronic Supplementary Information (ESI) available: [details of any supplementary information available should be included here]. See DOI: 10.1039/x0xx00000x

cross-linking.[33] The SCNP strategy demonstrates the feasibility of 3D assembly through noncovalent interactions, yet it lacks precise control over diverse secondary structure building elements. A universal platform is required to build 3D noncovalent polymeric architectures with well-defined local secondary and tertiary structural elements.

In this contribution, we report a side-chain functionalized helical polymer as a key building block for the formation of complex 3D materials, in particular supramolecular brush copolymers. Poly(isocyanide) (**PIC**) based on chiral menthyl-ester aryl isocyanides is known to fold into static helical polymers with preferred handedness and high helix inversion barrier due to the presence of lone pairs and bulky side groups.[34] The helix sense can be retained when mixing with achiral aryl isocyanides with alkoxylcarbonyl groups at the *p*-positions.[35] Therefore, the use of metal catalyzed isocyanide polymerization with both chiral and achiral isocyanides should generate helical random copolymers with full control over basic polymer properties, including dispersity and molecular weights.[36,37] We synthesize helical **PIC** copolymers (***co*-PIC**) with dispersed pyridine functionalities along the side-chains by combining the chiral menthyl-ester isocyanide with an achiral pyridine functionalized isocyanide. The pyridinyl groups are capable of coordinating with palladated sulfur-carbon-sulfur (SCS) pincer complexes, allowing directional assembly of the polymer blocks. While several noncovalent interactions on helical side-chains have been reported, including host-guest interactions,[38,39] the use of metal coordination to derive complex structures from the side-chains of a helical **PIC** is yet to be explored. To demonstrate the potential of our strategy, we describe the formation of a supramolecular helical brush copolymer featuring coil-like poly(styrene) (**PS**) pendant chains end-functionalized with Pd^{II}-pincer complex.

Results and Discussion

Synthesis of side-chain functionalized helical polymer.

Scheme 1 depicts the synthesis of the pyridine functionalized aryl isocyanide, **5**, in three steps starting from the formation of aryl formamide (**2**) according to published protocols.[40] 4-Pyridinepropanol, **3**, is coupled to the formamide by Steglich esterification to produce **4**. Visualizing a triplet at δ ~4.0 ppm (ester-CH_2) in the ^{1}H NMR spectrum confirms the new ester formation. The short alkyl chain between the pyridine and the ester group provides spatial flexibility between the functional group and the polymer backbone. Then, **4** is converted to the corresponding isocyanide using phosphoryl chloride and triethylamine. Purification via column chromatography and recrystallization affords the final aryl isocyanide monomer that is stored in solution at 0 °C to minimize self-polymerization. The monomer is characterized by NMR and IR spectroscopies and high-resolution mass spectrometry (Supporting Information). A strong absorption band at 2120 cm^{-1} in the FT-IR spectrum corresponds to the formation of the isocyanide.

Controlled polymerization of the isocyanides is mediated by a Palladium-anisole initiator prepared according to published protocols.[41] We target a degree of polymerization of 30 with a ratio of chiral to achiral monomers of 20:10 (Fig. 1a). While the circular dichroism (CD) signal intensities change linearly with the percentage of chiral isocyanides,[36,37] this feed ratio ensures a stable helical backbone with a high percentage ~~ratio~~ of functional groups for further functionalization via self-assembly. Polymerizations are performed in THF at 55 °C for 16 hours. The disappearance of the isocyanide ν_{CN} band in FT-IR spectra confirms the complete consumption of the isocyanide monomers (Fig. S4). The resulting ***co*-PIC** is purified by precipitation in cold methanol for at least three times. The polymer displays monomodal distribution and a dispersity ($Đ$) of 1.44, as determined by size-exclusion chromatography (SEC) in DMF (Fig. 1b). The ^{1}H NMR spectrum of the polymer contains all respective polymer resonances (Fig. S5) including a broad

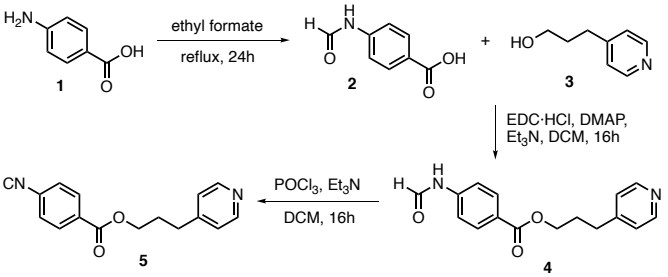

Scheme 1. Synthetic route toward the pyridine functionalized, achiral aryl isocyanide monomer.

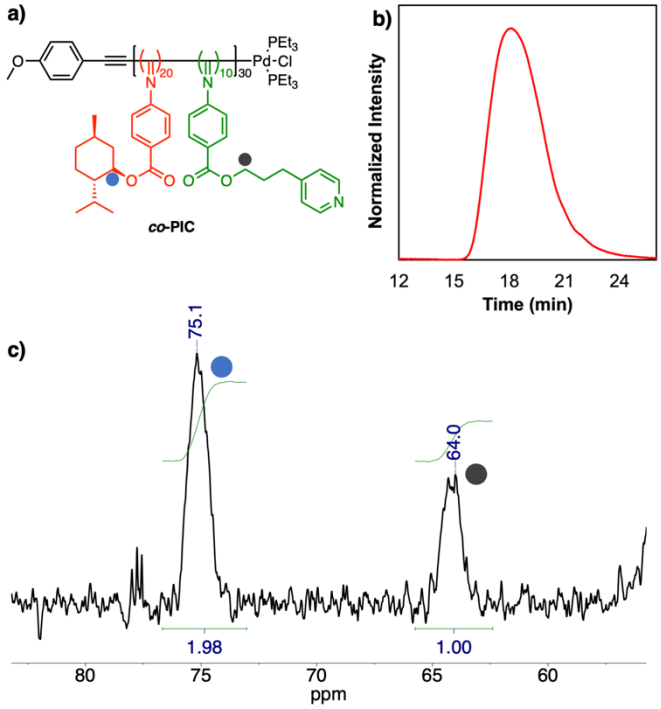

Figure 1. (a) Structure of the side-chain functionalized helical ***co*-PIC** with dots highlighting backbone signals of interest in the ^{13}C NMR spectrum. (b) SEC curve of ***co*-PIC** showing number average molecular weight (M_n) of 7,200 and dispersity ($Đ$) of 1.44. (c) Partial ^{13}C NMR spectrum (600 MHz, CD_2Cl_2) of ***co*-PIC** showing backbone signals from two types of monomers. Integration of these signals confirms that the ratio of chiral to achiral component is 2:1.

signal at δ 8.40 ppm that can be assigned to the *ortho* protons of the pyridine.

To gain quantitative insights of the polymer composition, ^{13}C NMR spectroscopy with inverse-gated-decoupling and prolonged relaxation delay has been proved useful.[42,43] The menthyl-ester isocyanide has a distinctive signal at δ 75-76 ppm, corresponding to the menthyl carbon adjacent to the carbonyl group (Fig. S3). Similarly, in the ^{13}C NMR spectrum, the signal of the carbon next to the carbonyl group in the pyridine containing **5** is located at δ 64-65 ppm (Fig. S2). We select these two distinctive signals for quantitative analysis since there is not any overlay with the neighboring peaks. A partial ^{13}C NMR spectrum with inverse-gated-decoupling, recorded in deuterated dichloromethane (CD_2Cl_2) is shown in Fig. 1c, where the two backbone signals of interest are present at δ 75.1 and 64.0 ppm. Integration of the two signals reveals a ratio of 1.98:1 that is very close to the 20:10 feed ratio, confirming the chemical composition of ***co*-PIC**.

Supramolecular assembly of co-PIC with Pd^{II}-pincer small molecule analog.

To investigate the metal coordination along the polymer side-chains, we first assemble a small molecule analog of the complimentary recognition unit, a Pd^{II}-SCS-pincer ligand **Pd-Pin** (Fig. 2a). The *t*-butyldimethylsilyl (TBS) protected pincer ligand is prepared according to published methods.[44] The use of the TBS protecting group prevents self-coordination between the metal center and the hydroxy group.[45] Upon metalation with $Pd(MeCN)_2Cl_2$, the signal of the hydrogen *para* to the aryl ring completely disappears in the ^1H NMR spectrum, confirming complete metalation of the ligand (Fig. S8). We mix ***co*-PIC** with **Pd-Pin** in CD_2Cl_2 with a molar ratio of 1:10 (1:1/pyridine:Pd^{II} pincer), followed by the addition of $AgBF_4$ to the physical mixture. $AgBF_4$ is an activating agent that triggers metal coordination by removing the Cl^- from the metal center and exposing the coordination site to pyridine molecules. After 30 minutes of stirring, we remove the insoluble AgCl by passing the solution through a syringe filter.

The metal coordination is tracked by ^1H NMR spectroscopy. As shown in Fig. 2b, we observe no shifts in the ^1H NMR spectra of the physical mixture, suggesting no interactions between the two species. Upon addition of $AgBF_4$, the resulting ^1H NMR spectrum displays the signature downfield shift of the α-pyridyl signal from δ 8.40 to 8.65 ppm. Furthermore, the aromatic proton signals on the pincer complex (β and γ in Fig. 2b) shift from 7.85 and 7.41 ppm, to 7.79 and 7.48 ppm, respectively. These signals are also broadened and lower in intensities. These diagnostic changes indicate metal coordination between ***co*-PIC** and Pd^{II} pincer complex.

UV-Vis spectroscopy is another powerful tool to track metal coordination owing to the signature metal-ligand charge transfer (MLCT) band of Pd^{II} pincer.[46] UV-Vis traces of the samples in solution are displayed in Fig. 3, where the MLCT band of **Pd-Pin** is located at 335 nm. The trace of the physical mixture

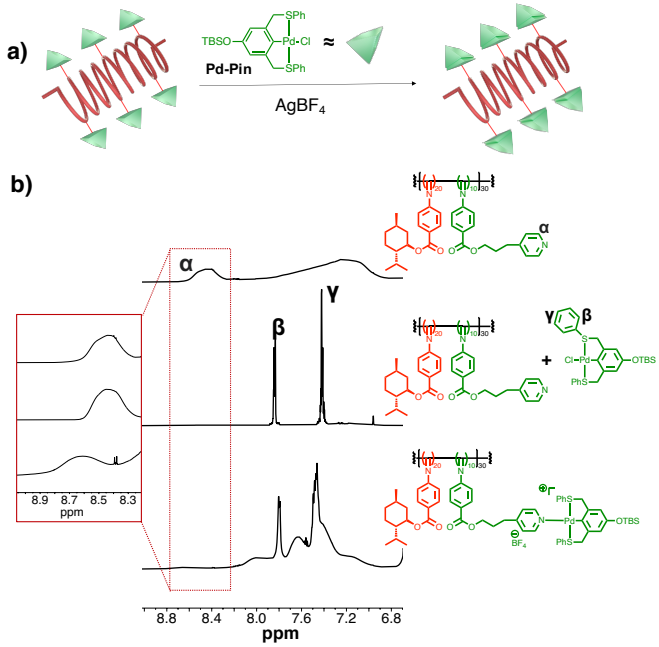

Figure 2. (a) Schematic representation of the side-chain supramolecular assembly of ***co*-PIC** and **Pd-Pin** complex. (b) Partial ^1H NMR (600 MHz) spectroscopic overlay of (top to bottom) **co-PIC**, physical mixture of ***co*-PIC** and **Pd-Pin,** and metal coordination assembly after $AgBF_4$ addition.

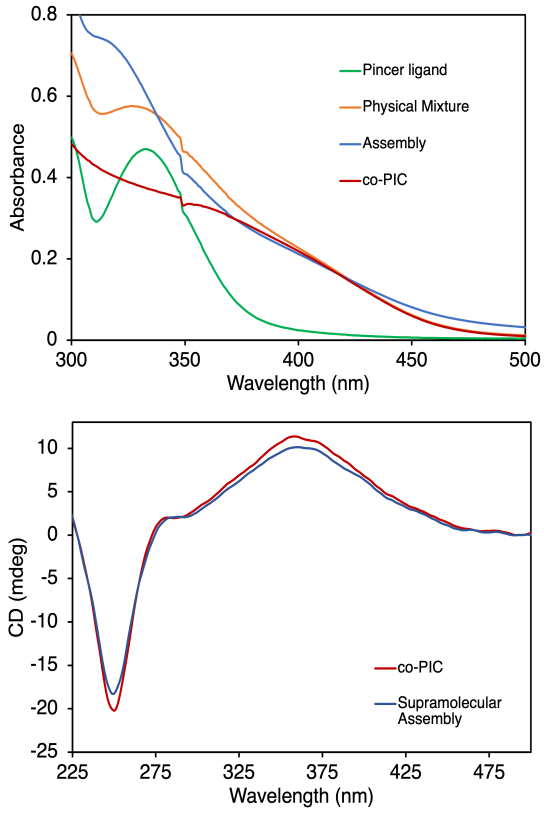

Figure 3. Spectroscopic analysis of ***co*-PIC** assembly with **Pd-Pin.** (top) UV-Vis traces of (green) **Pd-Pin**, (red) ***co*-PIC**, (orange) physical mixture, and (blue) metal coordination after $AgBF_4$ addition, recorded in DCE at 25 °C with [***co*-PIC**]=7.5 μM. (bottom) CD traces of (red) ***co*-PIC** and (blue) metal coordination after $AgBF_4$ addition, recorded in DCE at 25 °C with [***co*-PIC**]=7.5 μM.

is approximately the sum of two species and the MLCT band remains at 335 nm indicating no interaction between the two components. After $AgBF_4$ treatment, the band blueshifts to 310 nm, suggesting metal coordination. To prove that this blueshift is induced solely by the coordination of Pd^{II} pincer with the pyridyl end-groups, we perform ~~a~~ control experiments of **Pd-Pin** pyridine and $AgBF_4$ (Fig. S14). While there is no MLCT band change in the physical mixture of **Pd-Pin** and pyridine, mixing **Pd-Pin** and $AgBF_4$ results in a blueshift of the band to 325 nm. The blueshift to 310 nm is only observed in the assembly of **Pd-Pin** and pyridine at the presence of $AgBF_4$. Hence, the blueshift of MLCT band on UV-Vis spectroscopy suggests the metal coordination between pincer ligands and pyridine, thereby proving the assembly of ***co*-PIC** with **Pd-Pin**.

We then investigate the helicity of ***co*-PIC** using circular dichroism (CD) spectroscopy. The CD spectra are recorded in dichloroethane (DCE) at 7.5 μM with respect to the helical polymer. ***Co*-PIC** displays a broad band at λ 360 nm correlating to the n-π* transition of the C=N backbone, as well as a sharper peak at λ 250 nm corresponding to the π-π* transitions of the aryl rings.[34] Consistent with other examples,[35,37] the signal of ***co*-PIC** has an identical pattern but lower intensity compared to the **PIC** of menthyl-ester aryl isocyanides under the same concentrations. As shown in Fig. 3b, the CD traces before and after metal coordination are identical confirming that the side-chain assembly of *co*-PIC and Pd-Pin does not affect the helicity of the backbone.

Assembly of supramolecular brush copolymer with telechelic poly(styrene) side-chains.

Knowing that ***co*-PIC** is capable of side-chain metal coordination, we explore the formation of supramolecular brush copolymers via self-assembly by using a coil-like poly(styrene) functionalized with Pd^{II} pincer (**Pd-Pin-PS**). **Pd-Pin-PS** is prepared by atom transfer radical polymerization (ATRP) with a pincer functionalized initiator according to published procedures.[47] SEC analysis shows a dispersity of 1.23 with M_n of 4,000 (Fig. S11). We perform the assembly by mixing ***co*-PIC** and **Pd-Pin-PS** so that the molar ratio of pyridine and Pd^{II} pincer moieties is 1:1. The addition of excess $AgBF_4$ triggers metal coordination, resulting in the helical brush copolymer, ***co*-PIC-*brush*-Pd-Pin-PS**.

The metallosupramolecular assembly to form the brush copolymer is examined using ^1H NMR and UV-Vis spectroscopies. Fig. 4a shows the ^1H NMR spectra of a 1:10 physical mixture of ***co*-PIC** and **Pd-Pin-PS** (1:1 pyridine/Pd^{II} pincer) and the 1:10 mixture after the addition of $AgBF_4$. Consistent with observations made for the small molecule analogs, the α-pyridyl signal, originally appearing at δ 8.30-8.60 ppm, broadens and shifts to δ 8.38-8.82 ppm. The aromatic thioether proton signals on **Pd-Pin-PS**, broaden and shift from δ 7.84 and 7.43 ppm, to δ 7.78 and 7.47 ppm, respectively. The UV-Vis spectra of the physical mixture and assembled ***co*-PIC-*brush*-Pd-Pin-PS** are shown in Fig. 4b. We observe the blueshift of the MLCT band of **Pd-Pin-PS** from 335 nm to 310 nm. These

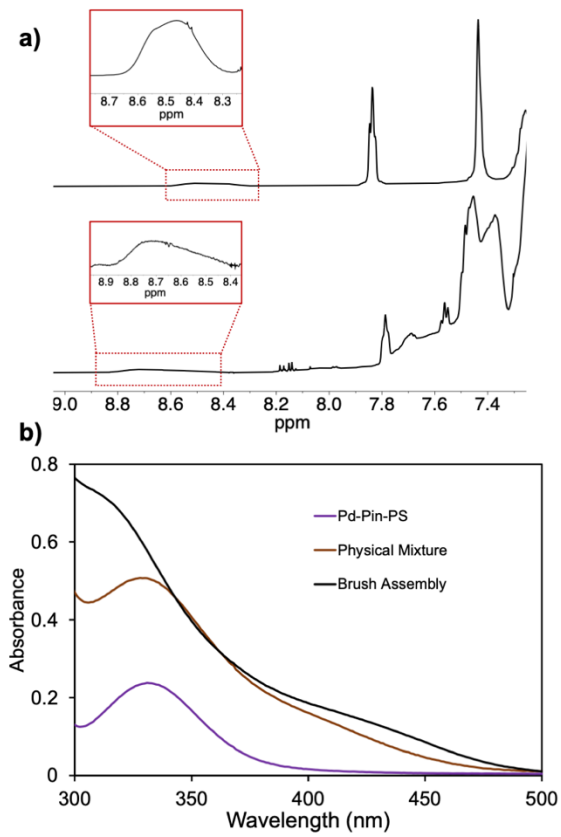

Figure 4. (a) ^1H NMR spectroscopic overlay of (top) physical mixture of ***co*-PIC** and **Pd-Pin-PS**, and (bottom) assembled ***co*-PIC-*brush*-Pd-Pin-PS** after $AgBF_4$ addition. (b) UV-Vis traces of (purple) **Pd-Pin-PS**, (brown) physical mixture of ***co*-PIC** and **Pd-Pin-PS**, and (black) assembled ***co*-PIC-*brush*-Pd-Pin-PS**. (DCE, 25 °C)

spectroscopic results provide evidence for metal coordination between the helical backbone and **PS** side-chains.

We use CD spectroscopy again to investigate the effect of brush copolymer formation on the helical conformation. As shown in Fig. 5, ***co*-PIC-*brush*-Pd-Pin-PS** displays signature Cotton effects of helical **PIC** at λ 360 and 250 nm, although there is an intensity decrease of the peak at λ 250 nm. Kanbayashi *et al.* reported that the electrostatic repulsion and bulky substituents on the side-chain can cause partial collapse of the helical structure.[38] In our case, we eliminate the contribution of electrostatic

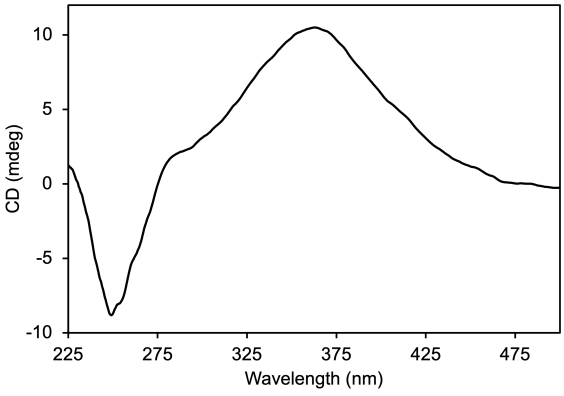

Figure 5. CD spectrum of ***co*-PIC-*brush*-Pd-Pin-PS**. (DCE, 25 °C)

repulsion, owing to the fact that the assembly with small-molecule analogs does not change the helical conformation. Thus, we hypothesize that the decrease in CD intensity is due to the presence of the bulky polymer side-chain. The helical backbone has to partially extend in order to accommodate the incoming polymeric brushes, resulting in decreased signal intensity at λ 250 nm. Despite this, the assembled structure still displays strong Cotton effects, suggesting that the **PIC** backbone maintains its helical conformation. We are actively investigating whether the steric ~~spatial~~ effect can be eliminated by introducing longer spacers between the pyridine functionalities and the aryl groups.

Unlike a physical mixture of individual polymer blocks, the brush copolymer assembled species should possess higher molecular weights, thereby inducing unique solution properties such as increased viscosityThe assembly via metal coordination can be characterized by comparing the solution viscosities before and after triggering the pincer complexation.[48] Viscosities of individual polymer blocks and the assembled brush copolymer are obtained in chloroform at room temperature with a Cannon-Ubbelohde viscometer. The specific viscosity (η_{sp}) of ***co*-PIC-*brush*-Pd-Pin-PS** increases in comparison to the individual blocks (Fig. 6, top). Compared to the viscosity measurements for the linear block copolymer assemblies, we observe larger specific viscosity changes.[16,17] This correlates to a significant increase in molecular weight, suggesting the presence of the supramolecular brush copolymer.

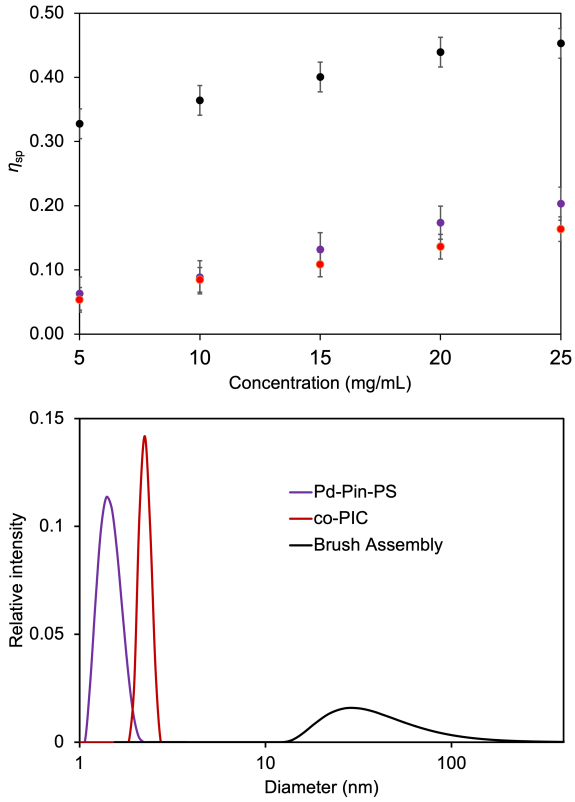

Figure 6. Characterizing the brush copolymer assembly by measuring (top) specific viscosity (η_{sp}) in $CHCl_3$ and (bottom) hydrodynamic radii (R_h) in DMSO; (red) ***co*-PIC**, (purple) **Pd-Pin-PS**, and (black) supramolecular brush assembly.

The bulk structure of the supramolecular assembly can be further analyzed by tracking the hydrodynamic radii (R_h) changes through dynamic light scattering (DLS). DLS data is obtained from an LS spectrometer with CONTIN fitting algorithm.[49,50] The bottom of Fig. 6 depicts the size distributions of homopolymers and assembled brush structures. The mean R_h of **Pd-Pin-PS** is 2 nm, which is smaller than the results from **PS** standard samples at similar molecular weight (Fig. S17). The solvent and the presence of telechelic pincer complex could have caused this minor discrepancy. The ***co*-PIC** displays a slightly larger R_h (2.2 nm) due to its higher molecular weight yet more compact conformation. The assembled brush copolymer records a dramatic increase in R_h (~60 nm) with a positively skewed distribution. Similar size increases have been reported for covalent grafting-onto and grafting-from linear brush copolymers.[51,52] Owing to the high local concentration of tethered chains, the grafted chains are forced to extend away around the polymer backbone, resulting in larger R_h and wider size distributions.

The significant increase in hydrodynamic volume of the brush copolymers suggests the presence of microphase separation between the polymer blocks.[53–55] This leads us to investigate the solid state properties of the metallosupramolecular brush assembly. The behavior is visualized by atomic force microscopy (AFM), where a lamellar structure with alternating bright and dark bands is observed in the brush copolymer assembly (Figure S20). This pattern is not captured in the AFM images of individual polymer blocks (Figures S21, 22) is most likely induced by the supramolecular assembly. Thus, in addition to ^{1}H NMR and UV-Vis spectroscopies, viscometry, DLS and AFM measurements support the formation of a supramolecular brush copolymer.

We further evaluate the solid-state assemblies using wide-angle X-ray scattering (WAXS). ***Co*-PIC**, **Pd-Pin-PS** and brush copolymer samples are mounted on silicon wafer as thin films for measurement. As shown in Fig. 7, the patterns of the homoblocks display broad bands, indicative of amorphous film formation. A bright peak appears in the wide-angle region of the brush copolymer assembly. The Bragg diffraction at 2ϑ = 38.2° correlates well to the Palladium-ligand bond in the pincer complex (2.36 Å).[45,56] The phase segregation between the backbone and side-chains can induce the transformation from amorphous, disordered homoblocks to the semi-crystalline morphology.[57] Therefore, the solid state studies strongly suggest the formation of an ordered arrangement of the metallosupramolecular brush species.

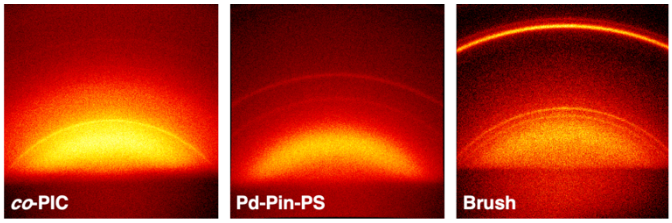

Figure 7. Two-dimensional diffraction patterns of (left to right) ***co*-PIC**, **Pd-Pin-PS**, and brush assembly. The bright peak at wide-angle area in the brush assembly suggests the formation of long-range ordered structures.

Conclusions

In summary, we report a methodology for the synthesis of side-chain functionalized helical polymers. A pyridinyl isocyanide is copolymerized with a chiral menthyl-ester isocyanide to form one-handed preferred helical random copolymers containing pyridine groups in the side-chains. The pyridinyl functional groups can participate in metal coordination with Pd^{II}-pincer complexes, as evidenced by ^{1}H NMR and UV-Vis spectroscopies. Using Pd^{II}-pincer functionalized telechelic poly(styrene), our methodology allows for the assembly of a supramolecular brush copolymer with a helical backbone. ^{1}H NMR and UV-Vis spectroscopies confirm the metal coordination. Viscometry and DLS verify the formation of a large polymeric ensemble in solution, with the presence of microphase separation, proving the successful preparation of a supramolecular brush copolymer. Our methodology leaps beyond main-chain supramolecular assembly, enabling the design of complex 3D materials. We envision this strategy as an expansion to the platform of building diverse architectures and fabricating functional materials.

Conflicts of interest

There are no conflicts to declare.

Acknowledgements

The authors acknowledge financial support from the National Science Foundation under award number CHE-1902917. We thank Dr. Joel Tang for the quantitative ^{13}C NMR spectroscopy analysis. We thank Hengyu Zhou for help in obtaining the AFM images and Dr. Chunhua Hu for his contribution to the X-ray measurements. The authors acknowledge the use of shared facilities provided through the Materials Research Science and Engineering Center (MRSEC) program of the National Science Foundation under Award Number DMR-1420073.

Notes and references

1 C. B. Thompson and L. T. J. Korley, 100th Anniversary of Macromolecular Science Viewpoint: Engineering Supramolecular Materials for Responsive Applications—Design and Functionality, *ACS Macro Lett.*, 2020, **9**, 1198–1216.

2 R. Scott Lokey and B. L. Iverson, Synthetic molecules that fold into a pleated secondary structure in solution, *Nature*, 1995, **375**, 303–305.

3 S. H. Gellman, Foldamers: A Manifesto, *Acc. Chem. Res.*, 1998, **31**, 173–180.

4 C. B. Anfinsen, Principles that Govern the Folding of Protein Chains, *Science*, 1973, **181**, 223–230.

5 B. Lewandowski, G. De Bo, J. W. Ward, M. Papmeyer, S. Kuschel, M. J. Aldegunde, P. M. E. Gramlich, D. Heckmann, S. M. Goldup, D. M. D'Souza, A. E. Fernandes and D. A. Leigh, Sequence-Specific Peptide Synthesis by an Artificial Small-Molecule Machine, *Science*, 2013, **339**, 189–193.

6 A. Aliprandi, M. Mauro and L. De Cola, Controlling and imaging biomimetic self-assembly, *Nat. Chem.*, 2016, **8**, 10–15.

7 Z. Dong, Q. Luo and J. Liu, Artificial enzymes based on supramolecular scaffolds, *Chem. Soc. Rev.*, 2012, **41**, 7890-7908.

8 S. Kassem, T. van Leeuwen, A. S. Lubbe, M. R. Wilson, B. L. Feringa and D. A. Leigh, Artificial molecular motors, *Chem. Soc. Rev.*, 2017, **46**, 2592–2621.

9 A. Ryabchun, F. Lancia, J. Chen, D. Morozov, B. L. Feringa and N. Katsonis, Helix Inversion Controlled by Molecular Motors in Multistate Liquid Crystals, *Adv. Mater.*, 2020, **32**, 2004420.

10 A. Croom, R. Tarallo and M. Weck, End-group functionalization and postpolymerization modification of helical poly(isocyanide)s, *J. Polym. Sci., Part A: Polym. Chem.*, 2016, **54**, 2766–2773.

11 E. Elacqua, A. Croom, D. S. Lye and M. Weck, Coil-helix and sheet-helix block copolymers via macroinitiation from telechelic ROMP polymers, *J. Polym. Sci., Part A: Polym. Chem.*, 2017, **55**, 2991–2998.

12 S. K. Pomarico, D. S. Lye, E. Elacqua and M. Weck, Synthesis of sheet-coil-helix and coil-sheet-helix triblock copolymers by combining ROMP with palladium-mediated isocyanide polymerization, *Polym. Chem.*, 2018, **9**, 5655–5659.

13 T. Nakano and Y. Okamoto, Synthetic Helical Polymers: Conformation and Function, *Chem. Rev.*, 2001, **101**, 4013–4038.

14 A. Croom, K. B. Manning and M. Weck, Supramolecular Helix–Helix Block Copolymers, *Macromolecules*, 2016, **49**, 7117–7128.

15 E. Elacqua, A. Croom, K. B. Manning, S. K. Pomarico, D. Lye, L. Young and M. Weck, Supramolecular Diblock Copolymers Featuring Well-defined Telechelic Building Blocks, *Angew. Chem. Int. Ed.*, 2016, **55**, 15873–15878.

16 R. Deng, M. Milton, S. K. Pomarico and M. Weck, Synthesis of a heterotelechelic helical poly(methacrylamide) and its incorporation into a supramolecular triblock copolymer, *Polym. Chem.*, 2019, **10**, 5087–5093.

17 E. Elacqua, K. B. Manning, D. S. Lye, S. K. Pomarico, F. Morgia and M. Weck, Supramolecular Multiblock Copolymers Featuring Complex Secondary

Structures, *J. Am. Chem. Soc.*, 2017, **139**, 12240–12250.

18 E. Elacqua, D. S. Lye and M. Weck, Engineering Orthogonality in Supramolecular Polymers: From Simple Scaffolds to Complex Materials, *Acc. Chem. Res.*, 2014, **47**, 2405–2416.

19 K. Maeda, S. Wakasone, K. Shimomura, T. Ikai and S. Kanoh, Chiral Amplification in Polymer Brushes Consisting of Dynamic Helical Polymer Chains through the Long-Range Communication of Stereochemical Information, *Macromolecules*, 2014, **47**, 6540–6546.

20 K. Maeda, S. Wakasone, K. Shimomura, T. Ikai and S. Kanoh, Helical polymer brushes with a preferred-handed helix-sense triggered by a terminal optically active group in the pendant, *Chem. Commun.*, 2012, **48**, 3342.

21 R. Baumgartner, H. Fu, Z. Song, Y. Lin and J. Cheng, Cooperative polymerization of α-helices induced by macromolecular architecture, *Nat. Chem.*, 2017, **9**, 614–622.

22 N. Liu, C.-H. Ma, R.-W. Sun, J. Huang, C. Li and Z.-Q. Wu, Facile synthesis and chiral recognition of block and star copolymers containing stereoregular helical poly(phenyl isocyanide) and polyethylene glycol blocks, *Polym. Chem.*, 2017, **8**, 2152–2163.

23 M. Sato, T. Kato, H. Shimamoto, K. Kamitani, N. Ohta, T. Hirai and A. Takahara, Design of High-Density Helical Polymer Brush on Silica Nanoparticles for the Size Recognition of Fullerene Molecules, *ACS Macro Lett.*, 2018, **7**, 148–152.

24 Y. Li, L. Xu, S. Kang, L. Zhou, N. Liu and Z. Wu, Helicity- and Molecular-Weight-Driven Self-Sorting and Assembly of Helical Polymers towards Two-Dimensional Smectic Architectures and Selectively Adhesive Gels, *Angew. Chem. Int. Ed.*, 2021, **60**, 7174–7179.

25 L. Xu, C. Wang, Y. Li, X. Xu, L. Zhou, N. Liu and Z. Wu, Crystallization-Driven Asymmetric Helical Assembly of Conjugated Block Copolymers and the Aggregation Induced White-light Emission and Circularly Polarized Luminescence, *Angew. Chem. Int. Ed.*, 2020, **59**, 16675–16682.

26 Y.-X. Su, L. Xu, X.-H. Xu, X.-H. Hou, N. Liu and Z.-Q. Wu, Controlled Synthesis of Densely Grafted Bottlebrushes That Bear Helical Polyisocyanide Side Chains on Polyisocyanide Backbones and Exhibit Greatly Increased Viscosity, *Macromolecules*, 2020, **53**, 3224–3233.

27 W.-B. Liu, X.-H. Xu, S.-M. Kang, X. Song, L. Zhou, N. Liu and Z.-Q. Wu, Bottlebrush Polymers Carrying Side Chains on Every Backbone Atom: Controlled Synthesis, Polymerization-Induced Emission, and Circularly Polarized Luminescence, *Macromolecules*, 2021, acs.macromol.1c00016.

28 E. Elacqua, G. T. Geberth, D. A. Vanden Bout and M. Weck, Synthesis and folding behaviour of poly(p-phenylene vinylene)-based β-sheet polychromophores, *Chem. Sci.*, 2019, **10**, 2144–2152.

29 M. Weck, Side-chain functionalized supramolecular polymers, *Polym. Int.*, 2007, **56**, 453–460.

30 S. Chen, N. Mahmood, M. Beiner and W. H. Binder, Self-Healing Materials from V- and H-Shaped Supramolecular Architectures, *Angew. Chem. Int. Ed.*, 2015, **54**, 10188–10192.

31 Y. Takashima, K. Otani, Y. Kobayashi, H. Aramoto, M. Nakahata, H. Yamaguchi and A. Harada, Mechanical Properties of Supramolecular Polymeric Materials Formed by Cyclodextrins as Host Molecules and Cationic Alkyl Guest Molecules on the Polymer Side Chain, *Macromolecules*, 2018, **51**, 6318–6326.

32 J.-F. Lutz, J.-M. Lehn, E. W. Meijer and K. Matyjaszewski, From precision polymers to complex materials and systems, *Nat. Rev. Mater.*, 2016, **1**, 16024.

33 O. Altintas, M. Artar, G. ter Huurne, I. K. Voets, A. R. A. Palmans, C. Barner-Kowollik and E. W. Meijer, Design and Synthesis of Triblock Copolymers for Creating Complex Secondary Structures by Orthogonal Self-Assembly, *Macromolecules*, 2015, **48**, 8921–8932.

34 E. Schwartz, M. Koepf, H. J. Kitto, R. J. M. Nolte and A. E. Rowan, Helical poly(isocyanides): past, present and future, *Polym Chem*, 2011, **2**, 33–47.

35 F. Takei, K. Onitsuka and S. Takahashi, Induction of Screw-Sense in Poly(isocyanide)s by Random Copolymerization between Chiral and Achiral Isocyanides Using Pd-Pt μ-Ethynediyl Dinuclear Complex as an Initiator, *Polym. J.*, 2000, **32**, 524-526.

36 F. Takei, K. Onitsuka, S. Takahashi, K. Terao and T. Sato, Control of Helical Structure in Random Copolymers of Chiral and Achiral Aryl Isocyanides Prepared with Palladium−Platinum μ-Ethynediyl Complexes, *Macromolecules*, 2007, **40**, 5245–5254.

37 S. Jimaja, Y. Xie, J. C. Foster, D. Taton, A. P. Dove and R. K. O'Reilly, Functional nanostructures by NiCCo-PISA of helical poly(aryl isocyanide) copolymers, *Polym. Chem.*, 2021, **12**, 105-112.

38 N. Kanbayashi, S. Tokuhara, T. Sekine, Y. Kataoka, T. Okamura and K. Onitsuka, Synthesis of helical polyisocyanides bearing aza-crown ether groups as

pendant, *J. Polym. Sci., Part A: Polym. Chem.*, 2018, **56**, 496–504.

39 F. Freire, E. Quiñoá and R. Riguera, Supramolecular Assemblies from Poly(phenylacetylene)s, *Chem. Rev.*, 2016, **116**, 1242–1271.

40 A. Xu, G. Hu, Y. Hu, X. Zhang, K. Liu, G. Kuang and A. Zhang, Remarkable Structure Effects on Chiroptical Properties of Polyisocyanides Carrying Proline Pendants, *Chem. - Asian J.*, 2013, **8**, 2003–2014.

41 Y.-X. Xue, J.-L. Chen, Z.-Q. Jiang, Z. Yu, N. Liu, J. Yin, Y.-Y. Zhu and Z.-Q. Wu, Living polymerization of arylisocyanide initiated by the phenylethynyl palladium(II) complex, *Polym Chem*, 2014, **5**, 6435–6438.

42 X. Qiu, D. Redwine, G. Gobbi, A. Nuamthanom and P. L. Rinaldi, Improved Peak Assignments for the ^{13} C NMR Spectra of Poly(ethylene- *co* -1-octene)s, *Macromolecules*, 2007, **40**, 6879–6884.

43 P. Giraudeau and E. Baguet, Improvement of the inverse-gated-decoupling sequence for a faster quantitative analysis of various samples by 13C NMR spectroscopy, *J. Magn. Reson.*, 2006, **180**, 110–117.

44 J. M. Pollino and M. Weck, Supramolecular Side-Chain Functionalized Polymers: Synthesis and Self-Assembly Behavior of Polynorbornenes Bearing PdII SCS Pincer Complexes, *Synthesis*, 2002, **2002**, 1277–1285.

45 N. C. Mehendale, M. Lutz, A. L. Spek, R. J. M. Klein Gebbink and G. van Koten, Self-assembly of para-OH functionalized ECE-metalated pincer complexes, *J. Organomet. Chem.*, 2008, **693**, 2971–2981.

46 I. Davidi, A. Semionov, D. Eisenberg, G. Goobes and R. Shenhar, Mesomorphic behavior induced by stacking interactions between poly(2-vinyl pyridine) and palladium pincer surfactants in the solid state, *Soft Matter*, 2012, **8**, 7393-7401.

47 D. S. Lye, Y. Xia, M. Z. Wong, Y. Wang, M.-P. Nieh and M. Weck, ABC Supramolecular Triblock Copolymer by ROMP and ATRP, *Macromolecules*, 2017, **50**, 4244–4255.

48 W. C. Yount, D. M. Loveless and S. L. Craig, Strong Means Slow: Dynamic Contributions to the Bulk Mechanical Properties of Supramolecular Networks, *Angew. Chem. Int. Ed.*, 2005, **44**, 2746–2748.

49 A. Scotti, W. Liu, J. S. Hyatt, E. S. Herman, H. S. Choi, J. W. Kim, L. A. Lyon, U. Gasser and A. Fernandez-Nieves, The CONTIN algorithm and its application to determine the size distribution of microgel suspensions, *J. Chem. Phys.*, 2015, **142**, 234905.

50 S. W. Provencher, A constrained regularization method for inverting data represented by linear algebraic or integral equations, *Comput. Phys. Commun.*, 1982, **27**, 213–227.

51 H. Lee, K. Matyjaszewski, S. Yu-Su and S. S. Sheiko, Hetero-Grafted Block Brushes with PCL and PBA Side Chains, *Macromolecules*, 2008, **41**, 6073–6080.

52 J. Pyun, T. Kowalewski and K. Matyjaszewski, Synthesis of Polymer Brushes Using Atom Transfer Radical Polymerization, *Macromol. Rapid Commun.*, 2003, **24**, 1043–1059.

53 S. K. Yang, A. V. Ambade and M. Weck, Supramolecular Alternating Block Copolymers via Metal Coordination, *Chem. - Eur. J.*, 2009, **15**, 6605–6611.

54 S. Eggers, F. Lauterbach and V. Abetz, Synthesis and self-assembly of high molecular weight polystyrene-block-poly[2-(N-morpholino)ethyl methacrylate]: A story about microphase separation, amphiphilicity, and stimuli-responsivity, *Polymer*, 2016, **107**, 357–367.

55 E. Brunner, K. Lutz and M. Sumper, Biomimetic synthesis of silica nanospheres depends on the aggregation and phase separation of polyamines in aqueous solution, *Phys. Chem. Chem. Phys.*, 2004, **6**, 854-857.

56 C. A. Kruithof, H. P. Dijkstra, M. Lutz, A. L. Spek, R. J. M. K. Gebbink and G. van Koten, X-Ray and NMR Study of the Structural Features of SCS-Pincer Metal Complexes of the Group 10 Triad, *Organometallics*, 2008, **27**, 4928–4937.

57 S. Chen and W. H. Binder, Dynamic Ordering and Phase Segregation in Hydrogen-Bonded Polymers, *Acc. Chem. Res.*, 2016, **49**, 1409–1420.

